Laser metrology concept consolidation for NGGM

Laser metrology concept consolidation for NGGM

K. Nicklaus[1], S. Cesare[2], L. Massotti[3], L. Bonino[2], S. Mottini[2], M. Pisani[4], P. Silvestrin[3]

[1] SpaceTech GmbH, Seelbachstr. 13, 88090 Immenstaad, Germany [2] Thales Alenia Space Italia S.p.A., Strada Antica di Collegno, 253, 10146 Torino, Italy [3] ESA/ESTEC, Keplerlaan 1, PO Box 299, 2200 AG Noordwijk, NL, The Netherlands [4] INRIM, Strada delle Cacce, 91, 10135 Torino, Italy

Abstract

The measurement of the static and temporal variation of Earth's gravity field yields important information on water storage, seasonal and sub-seasonal water cycles, their impact on water levels and delivers key data to Earth's climate models. The satellite missions GOCE (ESA), GRACE (US-GER) and just recently GRACE Follow-On (US-GER) resulted in a significant improvement on our understanding of the system Earth. To further improve the measurement accuracy of the time-variable gravity field, ESA is investigating the concept of a 'Next Generation Gravity Mission' (NGGM), consisting of two pairs of satellites and a heterodyne laser interferometer for inter-satellite ranging. Based on the heritage of the development of the laser ranging interferometer for GRACE Follow-On and the former and ongoing studies for NGGM, two schemes for the Laser Metrology Instrument (LMI) for NGGM, namely the transponder and the retroreflector scheme have been investigated and are presented in this paper. The results include the instrument ranging performance analyses, the laser link acquisition, an instrument reliability assessment and redundancy approach as well as the Technology Readiness Level assessment of the individual instrument units.

1 Introduction

The measurement of Earth's static and variable gravity fields by satellite missions has improved significantly over the last decades, see e.g., [1–7], providing a continuously improved knowledge on both the static and the temporally varying gravity field. With GRACE and GRACE Follow-On, two missions have been implemented to measure the temporal variation of Earth's gravity field. Figure 1 illustrates the measurement principle: two satellites are following each other on the same orbit about 100–300 km apart. The distance between the two satellites changes due to differences of the gravitational forces g_1 and g_2, as well as of the residual air drag forces F_{D1} and F_{D2} acting on the individual satellites. The distance changes Δd are measured interferometrically. To derive the gravity component of the distance variation, the air drag component is obtained measuring the non-gravitational acceleration on each satellite and subtracted from the interferometer ranging signal [8]. On GRACE the variation of the inter-satellite distance was measured by microwave inter-satellite ranging system (MWI) to approximately 1-10µm @ 10Hz [1] and enabled a gravity field recovery to about 1 mm geoid error with 350 km spatial resolution [5]. On GRACE Follow-On, which has been launched May 22nd 2018, in addition to the MWI a heterodyne Laser Ranging Interferometer (LRI) is embarked as an experiment to demonstrate the capability of this system to improve the ranging accuracy by at least one order of magnitude [9–12]. The LRI is implemented as an off-axis transponder configuration. A highly stable laser beam emitted from one spacecraft is received on the second spacecraft, where a laser is phase locked to the received signal. This signal is then sent back to the first spacecraft, where the variation of the phase angle—due to the relative motion of the two spacecraft—is measured with a phasemeter, similarly to the approach foreseen for LISA [13, 14].

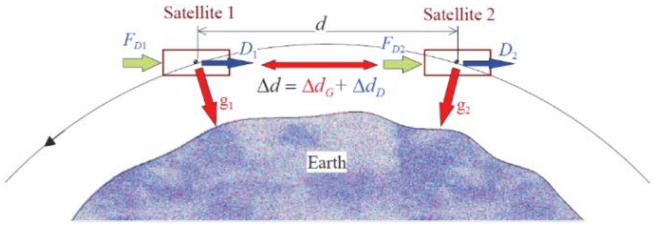

Fig. 1 Measurement principle of the Earth's gravity field measurement by satellite-to-satellite tracking

The achievable measurement resolution is a small fraction of the laser wavelength. First in-orbit measurement data of the LRI indicate excellent performance down to 1nm/√Hz at a Fourier frequency of 100 mHz [7]. The data is now provided openly on a monthly basis [15]. However, due to the limited accelerometer performance and the measurement taken by a single satellite pair in polar orbit, the gravity field recovery is limited to a performance only slightly better than the MWI and similar to GRACE [6].

2 NGGM top level mission and LMI requirements

With the (provisionally called) NGGM mission, ESA aims to achieve an improved measurement of the variable Earth's gravity field, in terms of temporal and spatial resolution, to better track the mass changes within the planet "system". The stated objective is to measure the geoid with 1 mm accuracy at 3-day intervals with < 500 km spatial resolution, and at 10-day intervals with < 150 km spatial resolution, over a time span of at least 7 years [16].

A promising mission scenario to achieve this goal is a satellite mission consisting of two pairs of satellites in a so called Bender configuration [17–19]. One pair flies on a polar orbit with about 90° inclination, while a second pair flies on 60–70° inclination, at an altitude range between 340 and 380 km and with an inter-satellite distance of about 100 km between the two satellites of each pair. The heterodyne laser interferometer is foreseen as the main instrument. The top-level requirements for the laser interferometer were derived along the study: Table 1 lists the key mission parameters, the expected satellite environment and the main LMI performance requirements which are the basis for the mission design. Figure 2 shows the ranging noise requirement and goal of NGGM in comparison to GRACE FO, as well as the measured thermal environment from the GOCE gradiometer, which serves as input for the definition of the thermal environment for the LMI. Figure 3 shows the result of the preliminary simulation of a satellite pointing performance, which stays below 2μrad/√HzxNSF(*f*) in the science measurement frequency band which is used for the performance analysis. The simulation assumes the absence of any beam steering mirror, and the pointing capability provided by the satellite platform.

Table 1 Key NGGM mission parameter and requirements relevant for the LMI

Parameter	Value	Comment
Mission parameters and LMI requirements		
Inter-satellite distance	100 km	
Orbit height	340–380 km	
Inter-satellite ranging noise (single link)	$\tilde{x}_{\text{thr}} \leq 20\frac{\text{nm}}{\sqrt{\text{Hz}}} x\,\text{NSF}(f)$ for $1x10^{-4}\text{Hz} < f < 1\,\text{Hz}$ $\tilde{x}_{\text{goal}} \leq 10\frac{\text{nm}}{\sqrt{\text{Hz}}} x\,\text{NSF}(f)$ for $1x10^{-4}\text{Hz} < f < 1\,\text{Hz}$	with $\text{NSF}(f) = \sqrt{1 + \left(\frac{10\text{mHz}}{f}\right)^2}$
Mission duration/LMI reliability	7 Years/87%	
Satellite environment		
Thermal noise around LMI units	$\tilde{T}_{\text{thr}} < 0.01\frac{\text{K}}{\sqrt{\text{Hz}}} x\,\text{NSF}(f)$ for $1x10^{-4}\text{Hz} < f < 1\,\text{Hz}$	Derived from GOCE thermal environment measurement data
Satellite pointing error in science mode	$\vartheta, \psi < 20\,\mu\text{rad}$	
Satellite pointing noise	$\tilde{\vartheta}, \tilde{\psi} < 2\frac{\mu\text{rad}}{\sqrt{\text{Hz}}}$ for $1x10^{-2}\text{Hz} < f < 1x10^{-1}\,\text{Hz}$ $\tilde{\vartheta}, \tilde{\psi} < 10\frac{\mu\text{rad}}{\sqrt{\text{Hz}}}$ for $1x10^{-3}\text{Hz} < f < 1x10^{-2}\,\text{Hz}$	$\tilde{\vartheta}$= pitch angle ψ= yaw angle
LMI unit requirements/performances		
Laser frequency noise	$\delta f \leq 40\frac{\text{Hz}}{\sqrt{\text{Hz}}} x\,\text{NSF}(f)$ for $1x10^{-4}\text{Hz} < f < 1\,\text{Hz}$	From HSL [32]
Laser RIN	$\text{RIN} \leq 10^{-3}\frac{\text{Hz}}{\sqrt{\text{Hz}}}\sqrt{1 + \left(\frac{10\text{mHz}}{f}\right)^4}$ for $1x10^{-4}\text{Hz} < f < 1\,\text{Hz}$	From HSL [32]

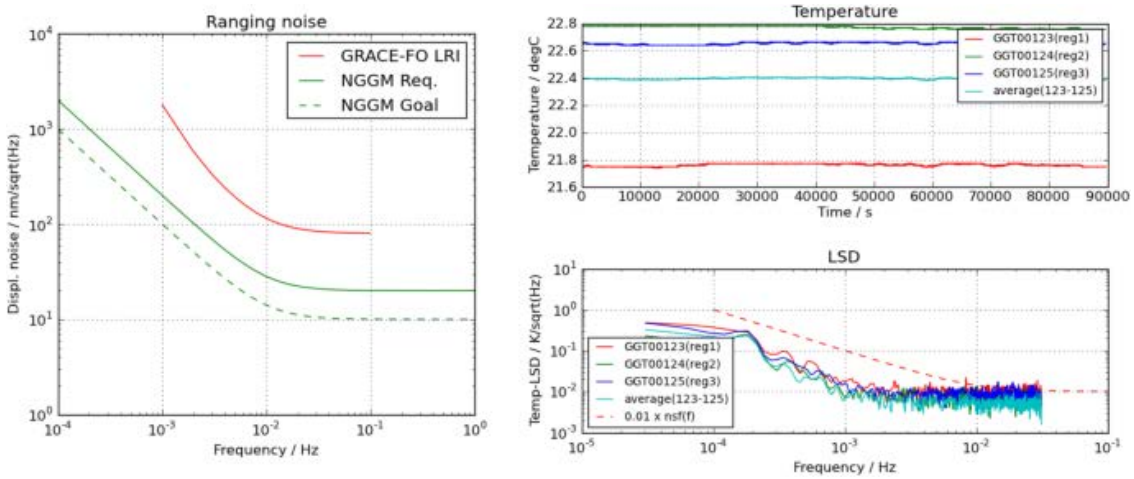

Fig. 2 Left: interferometer ranging noise requirements of NGGM and GRACE Follow-On; Right: GOCE gradiometer thermal environment

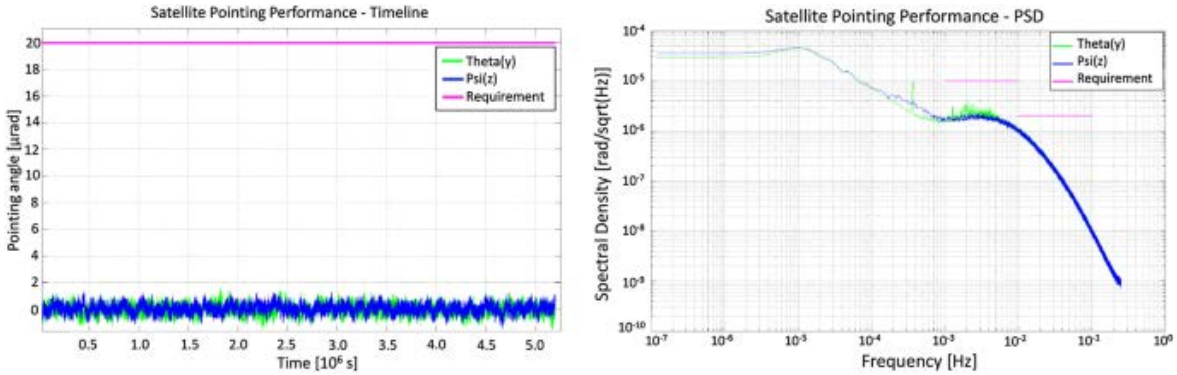

Fig. 3 Left: absolute satellite pointing error simulation; Right: satellite pointing noise simulation

The challenging ranging noise requirement leads to a range of interferometer design rules that have been originally been identified during the development of the LRI for GRACE FO, and that are also applicable to this development for NGGM, such as:

- The measurement needs to be performed from the center of mass (CoM) of satellite 1 to the CoM of the satellite 2 (as depicted in Fig. 1). For the assumed satellite pointing performance and to reach requested sensitivity to the tiny variations of the gravity filed anomalies, the position accuracy of the measurement reference points (materialised by retro-reflector vertex) with respect to the satellite CoM needs to be in the mm range.
- The number of optical elements and the propagation of the optical beams within material in the optical measurement path (namely the instrument optical bench) needs to be minimised. Optical surfaces orthogonal to the optical beam direction need to be avoided: firstly, to minimize stray light and secondly to minimize the noise coupling due to thermal effects into the pathlength measurement.
- Due to the unequal arm length of the interferometer, the laser frequency noise is one of the main contributors to the interferometer performance and is the ultimate limit to the achievable ranging noise performances.

In addition, further considerations have been taken into account for the development of the interferometer schemes, such as the required power, LMI mass as well as the impact on the overall satellite system cost due to the individual accommodation of the different schemess into the spacecraft.

3 LMI instrument implemention schemes

We have studied and traded-off the two basics interferometer schemes, namely the optical transponder scheme as applied on GRACE-FO [7] and the enhanced retroreflector scheme, already investigated in former NGGM studies [20, 21]. The focus of our investigation lied on the assessment their general suitability, achievable performance, system level impacts and necessary further development for the laser interferometer for NGGM.

Both schemes rely on heterodyne interferometry and consist of very similar basic instrument units, with individual internal unit variations depending on the scheme. The key LMI units are described below.

The laser head (LH), consisting of a single frequency laser source, providing a fundamental mode Gaussian beam. The LH needs to provide an output power of 8 mW for the transponder scheme and 500 mW for the retroreflector scheme. The LH contains the laser electronics, including the drive electronics for the frequency stabilisation of the laser head to the optical cavity. The seed laser may be either a non-planar ring oscillator (NPRO), as used on GRACE Follow-On, providing 25 mW of output power [7], or an extended cavity diode laser (ECDL), e.g., based on the MILAS technology, which is currently being developed for space application, providing more than 500 mW of output power [22]. Depending on the derating strategy, approx. 250 mW are considered realistic for a space qualified module. The ECDL technology offers the benefit of significantly higher efficiency and output power but is not available as space qualified yet. In case of the retroreflector scheme, the LH, furthermore, contains a fibre amplifier and a frequency shifter to achieve the required optical output power of 500 mW and the offset frequency for the local oscillator signal.

The optical cavity (CAV), consisting of an Ultra-stable Fabry–Perot reference cavity, the fibre coupled EOM for Pound-Drever-Hall (PDH) control scheme, the coupling optics arm and the photoreceivers for the PDH control loop and potentially a vacuum pump. The cavity needs to be enclosed in thermal shielding to achieve the required high thermal stability to allow a frequency stabilisation of the laser to the single Hz/sqrt(Hz) level.

The optical bench assembly (OBA), consisting of the fibre-to-free space interface of the laser, means for beam clean-up, shaping and routing of the laser signal to the photoreceivers of the distant spacecraft, quadrant photoreceivers and the acquisition laser detector (ALD).

The retroreflector (RR), consisting of a three mirror retroreflector with its vertex located in the satellite center of mass (CoM). It routes, in off-axis configuration, the transmitted beam from the optical bench to the other spacecraft. Placing the vertex of each RR into each satellite's CoM enables the LMI to measure the distance variation of the CoM of the two satellites to nm accuracy without the need to actually have a physical mirror in the CoM, which is the preferred position of the accelerometer test mass. For NGGM two accelerometers positioned symmetrically around the CoM are currently foreseen so that the CoM may also be directly accessible. The use of hollow retroreflectors properly oriented and coated with respect to the laser polarisation state ensures no depolarization upon reflection.

The instrument control unit (ICU), containing the data processing and TM/TC, the Interface to the OBC, the photoreceiver readout electronics, the phasemeter, the laser control electronics (on/off, frequency control, etc.), the cavity stabilisation control loop electronics and the link acquisition control loop.

The acquisition light source (ALS), consisting of a laser source with rather wide beam divergence of some mrad, acting as an "artificial guide star" to enable link acquisition (together with an Acquisition Laser Detector on the OBA).

Furthermore, baffles at various locations between the optical bench and the retroreflector in the satellite ensure the reduction of straylight and protect the free space beam path from any potential obstruction.

Please note, that the ALS and ALD are not strictly considered part of the LMI, but rather a separate system that allows pre-alignment of the two spacecraft to each other to enable the optical link. As they are nonetheless essential for the operation, the system is included in the overall discussion.

Figure 4 shows the basic implementations of both investigated instrument schemes, with red beams showing the base laser frequency beams and in green the frequency shifted beams. The operating principle of the LMI in science mode is as follows: the LH signal, stabilised to the ultra-stable reference cavity, is launched onto the optical bench and split up into a local oscillator and a transmit

beam by a beam splitter (BS). The imaging optics (L1 and L2) in front of the photoreceiver image the exit of the fibre collimator and the aperture, where the received beam from the other S/C enters the OBA onto the photoreceiver, thereby minimizing the effect of beam walk due to beam angle changes as well as phase errors due to diffraction effects of the baffles and entrance aperture. The compensation plate (CP) minimizes the ranging noise introduced by the beam splitter pointing noise. In case of the retroreflector scheme the local oscillator and the transmit laser signal are delivered separately to the optical bench and a second photoreceiver diode (PD1) serves as reference phase measurement to cancel out any phase fluctuation between the two laser signals introduced by the fibre, the frequency shifter and the fibre amplifier. Here, a small portion of the transmit signal transmits through beam splitter 1 (BS1) towards PD1 to enable the fibre phase fluctuation subtraction.

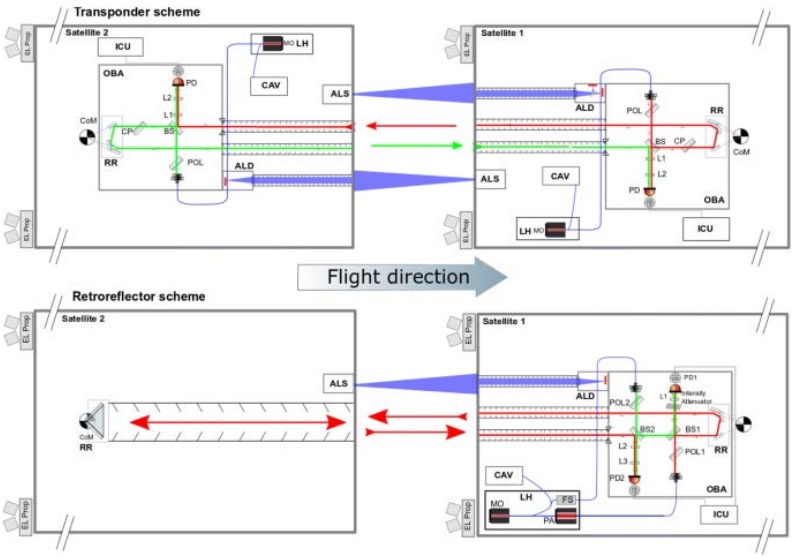

Fig. 4 Basic LMI-transponder (top) and LMI-retroreflector (bottom) schemes

Only the BS1 and CP (respectively, BS2 for the retroreflector scheme) are in the direct measurements path, in which any pathlength noise directly couples into the ranging performance. The noise of all other optical elements (from fibres-to-BS and BS-to-photoreceivers) is strongly suppressed due to common-mode effects or cancelled out by the fibre phase fluctuation subtraction. The transmit beam is then sent out to the second spacecraft, via the retroreflector. Then the second spacecraft reflects the beam back to the first one. Depending on the implemented scheme the beam reflection is done either directly using of a second passive retroreflector or by a setup identical to that one on the first spacecraft, where the laser is frequency offset locked to the incoming beam and its signal is sent back to the first spacecraft.

On the first spacecraft (S1), the received beam from the second spacecraft (S2) is superimposed with the local oscillator beam onto a quadrant photodiode whose signal is recorded by the phasemeter in the instrument control unit (ICU).

The main science signal of the instrument is the phase variation of the received signal relative to the local oscillator phase measured by the photoreceivers on the optical bench of Satellite 1, called the heterodyne signal. It contains the fixed frequency offset plus twice the Doppler shift due to the relative motion of the two spacecraft, expected in the order of some hundred kilohertz. To enable the required low measurement noise the phase measurement accuracy needs to be in the single mrad/sqrt(Hz) range. From this phase measurement, the accelerometer signals and potentially further calibrated signals, and background models (i.e., tidal models) the gravity field is ultimately derived [7, 19].

In addition, the phase differences between the individual quadrants of the photoreceivers are evaluated and utilized to measure the relative pointing and ultimately align the two spacecraft

towards each other with microrad precision. This differential wavefront sensing principle is described e.g. in [11].
Both schemes in principle enable an interferometric measurement from the CoM of one spacecraft to the CoM of the other spacecraft with the required “nanometer per root Hertz” precision. Both instrument schemes can be implemented with an on- or off-axis configuration concerning the separation of the outgoing (S1 → S2) and the incoming (S1 ← S2) laser beams. In the On-axis configuration as described e.g. in [21] the optical signal separation is achieved via a different polarisation status of the outgoing/incoming laser beam, while in the off-axis (also called “racetrack”) configuration—as implemented in GRACE FO—the beam separation is achieved via different optical paths travelled by the outgoing/incoming laser beams. For both schemes, we consider the off-axis variants superior due to less criticality with respect to polarisation, straylight, complexity of setup, number of optical elements in the beam path and no need to have direct access to the satellite CoM. Therefore, the two baselined solution for the study focussed on the off-axis instrument schemes. The configuration of these two has been optimized and traded against each other with respect to science performance, technical complexity, TRL, reliability, size, weight and power, impact of the accommodation on the spacecraft and LMI cost. Table 2 summarizes the key parameters and system aspects of the two interferometer schemes for which the comparison has been performed.

Table 2 Comparison of the two LMI Schemes

Criterion/parameter	LMI-transponder scheme (Racetrack)	LMI-Retroreflector scheme (Racetrack)
Optical and geometrical parameters		
Inter-satellite distance	Both: 100 km	
Laser power out laser head	25 mW, linear polarised	Transmit beam: 500 mW, Local oscillator beam: 25 mW, linear polarised
BS1/CP reflectivity	CP: 0.2%	BS1: 99%
BS2/BS reflectivity	BS: 90%	BS2: 90%
Loss due to molecular contamination per surface (high/low case)	0% / 5%	0% / 5%
Transmit Gaussian beam diameter	5 mm	5 mm
Beam divergence (high/low case)	142 µrad/163 µrad	142 µrad/163 µrad
Beam coalignment error (high case/low case)	0 µrad/40 µrad	0 µrad/40 µrad
Receive aperture diameter	8 mm	8 mm
Retroreflector free aperture and coalignment error on passive satellite	–	36 mm, 0–5 µrad
Free space Loss (for $d = 100$ km)	68—70 dB	105–109 dB
Received power from S2 (low—high) in received aperture	1.1–3.0 nW	1.8–5.6 pW
LMI system aspects		
Laser source	Single frequency laser (NPRO/ECDL)	Master oscillator power amplifier (single frequency NPRO/ECDL + Fibre amplifier), frequency shifter (AOM)
Laser source stabilisation	Both: Ultra-stable reference cavity	
Detection system	Evaluation of CW beam, Quadrant photo receivers, science mode beam pointing based on DWS signal	Evaluation of CW beam, Quadrant photo receivers, science mode beam pointing based on DWS signal, second quadrant photoreceiver as reference to calibrate out phase shifts in delivery fibre
Optical system	Both: only plane optics in performance critical path	
Mass and power		
Mass estimate	Approx. 43 kg (65 for fully redundant scheme)	Approx. 45 kg
Power estimate (science)	Approx. 65 W	Approx. 96 W
Power estimate (acquisition)	Approx. 74 W	Approx. 105 W

As stated, the proposed transponder scheme is very similar to the LRI of GRACE FO. The conceptual differences are the removal of the steering mirror on the optical bench in favour of a dedicated link acquisition system (consisting of the ALS and ALD) and laser beam pointing performed by spacecraft attitude control, as well as the higher level of instrument redundancy to achieve a higher reliability for the longer mission design lifetime. Both are described and justified in Sects. 5 and 6 below. Furthermore, the mechanical and physical implementation will differ due to satellites being specifically designed to accommodate the LMI as the main instrument, allowing e.g., a smaller beam separation and, therefore, a less demanding retroreflector design.

4 Performance analysis results

The LMI performance has been analysed including key laser interferometer noise contributors which are:

- Laser frequency noise
- Phasemeter ranging noise or heterodyne signal detection noise (such as shot noise, electronic noise, power noise, RIN and dark current in relation to the heterodyne signal amplitude)
- Thermal noise contribution of the retroreflector and of the optical bench
- 'Satellite induced' noises due to limited center of mass stability of the satellite
- Pointing noise of the satellite influencing the ranging, via the coupling to the path lengths on the OBA and RR
- Ranging errors due to wavefront planarity.

Table 3 lists all effect descriptions and the corresponding formulas. Yet to be analysed is the influence of straylight as well as potential cycle slip issues for the retroreflector scheme due to the low received signal.

Table 3 LMI Ranging Noise contributors

Parameter	Dependency/formula
Laser interferometer noise	
Laser frequency noise (from e.g., [23].)	$\tilde{x} = \frac{L}{\nu}\tilde{\nu}$ with $\tilde{x}$ being the ranging noise amplitude spectral density, L the baseline length between the two spacecraft, ν the laser frequency and $\tilde{\nu}$ the laser frequency amplitude spectral density
Heterodyne signal (from e.g., [23].)	$I(t) = \eta_{PD}\left[P_{lo} + P_{rec} + 2\sqrt{\eta_{het}P_{lo}P_{rec}}\cos(\omega_b t + \varphi)\right]$ with η_{PD} being the photodiode efficiency, η_{het} heterodyne efficiency, ω_b the angular frequency difference between the interfering beams and φ the averaged phase difference
Phasemeter ranging noise (from e.g., [23].)	$\Delta s_{pm} = \frac{\lambda}{2\pi}\frac{\text{noise}_{ph}}{I_{het\_rms}}$ $\text{noise}_{ph} = \sqrt{\text{noise}_{shot}^2 + \text{noise}_{el}^2 + \text{noise}_{RIN}^2}$ $I_{het_{rms}} = \eta_{PD}\sqrt{2\eta_{het}P_{lo}P_{rec}}$ With λ being the laser wavelength. The individual noise contributors are given below. Using sufficient power and a sufficiently stable laser source, Power noise and dark noise are so small, that they are omitted in the calculation
Shot noise (from e.g., [23].)	$noise_{shot} = \sqrt{2q_e\eta_{PD}(P_{rec} + P_{lo})}$ $\Delta s_{shot} = \frac{\lambda}{2\pi}\sqrt{\frac{q_e(P_{rec}+P_{lo})}{\eta_{PD}\eta_{het}P_{rec}P_{lo}}}$ Assuming $P_{lo} >> P_{rec}$, the shot noise induced pathlength noise is independent from P_{lo} and scales with $1/\sqrt{P_{rec}}$
Electronic noise (from e.g., [23].)	$\text{noise}_{el} = n_{el}$ $\Delta s_{el} = \frac{\lambda}{2\pi}\frac{n_{el}}{\eta_{PD}\sqrt{2\eta_{het}P_{rec}P_{lo}}}$ with n_{el} being the electronic noise of the photoreceiver. A typical value (taken from GRACE FO LRI) is n_{el}= 5 pA/√Hz. The electronic noise scales with $1/\sqrt{P_{rec}}$ and $1/\sqrt{P_{lo}}$ respectively
RIN (from e.g.,[23].)	$\text{noise}_{RIN} = \eta_{PD}(P_{rec} + P_{lo})\text{RIN}$ $\Delta s_{RIN} = \frac{\lambda}{2\pi}\frac{\text{noise}}{I_{het}} = \frac{\lambda}{2\pi}\frac{(P_{rec}+P_{lo})}{\sqrt{2\eta_{het}P_{rec}P_{lo}}}$ RIN The RIN of the laser source in the MHz range is assumed as -130 dB/√Hz (for the TESAT NPRO) above 1 MHz. The power noise scales with P_{lo} and $1/\sqrt{P_{rec}}$
Thermal noise of optical bench	Three contributors are entering the thermal noise of the optical bench: 1. Noise induced on the measurement path is caused mainly by the change of the refractive index and the CTE of BS1and 2, respectively the CP. Calculation via optical pathlength simulation 2. Common mode delivery paths (local oscillator and transm./rec. beam on the same path) enter with: Free space $\tilde{x}(f)_{fs-bs} = -\frac{2\pi fL\,\text{ad}}{c}\tilde{T}(f)$ Glass and fibre $\tilde{x}(f)_{\text{fiber}} = -\frac{2\pi fL(\frac{dn}{dT}+\alpha)d}{c}\tilde{T}(f)$ with α being the coefficient of thermal expansion, d the optical path length, f the measurement frequency and L the distance between the two spacecraft 3. Non common mode delivery paths: For any non-common mode path length noise in the delivery path, the path length noise directly enters the measurement performance with: $\tilde{x}(f)_{\text{delivery}} = \left(\frac{dn}{dT} + \alpha\right)d\,\tilde{T}(f)$ At the given environmental thermal noise, a noise of close to 10 nm/√Hz is introduced for every 10 cm of non-common mode path length for quartz glass and titanium material. Any non-common mode delivery path needs, therefore, to be minimized or calibrated out for not exceeding the allocations With these contributors and the thermal mass of the RR itself a performance of 1 nm/√Hz × NSF(f) was achieved even under the significantly worse thermal environment of GRACE FO of 0.3 K/√Hz × NSF(f) in the platform. This is taken as the upper limit also for the LMI
Thermal noise of retroreflector	The thermal noise of the retroreflector is given by the movement of the vertices under temperature noise. For GRACE FO a CRFP-Zerodur™ hybrid RR was designed with a longitudinal coupling factor of less than 400 nm/K. With this and the thermal mass of the RR itself a performance of 1 nm/√Hz × NSF(f) was achieved even under the significantly worse thermal environment of GRACE FO of 0.1 K/√Hz × NSF(f) in the accelerometer compartment. This is taken as the upper limit also for the LMI

Satellite and beam pointing induced noise	
Coupling of retroreflector vertex and satellite CoM with satellite pointing	The change of the optical pathlength due to one retroreflector is $\Delta OPL = 2\Delta y\delta\theta + 2\Delta z\delta\psi - \Delta x\psi^2 - 2\Delta y\delta\theta^2$ With $\Delta x, \Delta y, \Delta z$ being the vertex displacement of the RR in flight direction and transversal to it and $\delta\theta$ and $\delta\psi$ being the change in pitch and yaw angle. Allocating 4 nm/$\sqrt{\text{Hz}}$ x NSF(f) for pitch an yaw and using the given pointing requirement, leads to a required vertex accuracy of 0.14 mm per transversal axis $\Delta y, \Delta z$, while Δx is even for 5 mm displacement uncritical
Coupling of optical bench with satellite rotation	The optical pathlength on the optical bench changes with rotation due to the pathlength changes inside the beamplitters and compensation plate. Assuming a thickness of 7 mm, the change is given by 8.4 nm-θ [mrad] for rotation around z and 4.6 nm-ψ [mrad] for rotation around y. Assuming a worst case OBA misalignment of less than 10 mrad, the coupling is less than 100 µm/rad, corresponding to less than 1 nm/$\sqrt{\text{Hz}}$ for the given satellite pointing stability
Coupling of wavefront planarity—optical system quality	The wavefront planarity is limited by the design and manufacturing quality of the optical system. The ideal wavefront received by the spacecraft is a spherical wave with radius of the inter-satellite distance. In this ideal case rotation of the transmitting spacecraft does not lead to ranging errors. For a Gaussian beam the transmitted wavefront needs to be perfectly flat to achieve this goal. As any non-planar optics are a potential cause of defocus and spherical aberrations, the racetrack designs employ only plane optics, with the exception of the beam collimator that generates the initial beam at the required diameter. As analysed in the LRI for GRACE Follow-On, wavefront planarity errors are significantly reduced in the far field (from $\lambda/15$ PV@1e^2 diameter at the local spacecraft to $\lambda/200$ at a distance of 200 km). Assuming a reasonably flat phase front and a Gaussian beam, the ranging noise of this effect is expected to be negligible also for the target NGGM inter-satellite distance of 100 km For the received beam in addition to the wavefront planarity, diffraction effects by the limiting apertures need to be taken into account in the OBA and baffle design
Coupling of wavefront planarity—diffraction effects	Diffraction effects are caused by limiting apertures The optical design of the transmit beam paths ensures a free aperture of at least three times the Gaussian beam diameter for the transmitted beams to avoid clipping of the beam For the received beam, the apertures at the entrance of the spacecraft and on the optical bench are relevant. For the spacecraft entrance high Fresnel numbers (>>100) are assumed to avoid significant effects under pointing changes. The entrance aperture of the optical bench is imaged onto the photoreceiver to eliminate phase errors In the retroreflector scheme the beam clipping of the distant spacecraft causes phase-front errors. These phase errors are significant at the distant spacecraft (several π), but are also strongly reduced over 100 km propagation. Performing a physical optics propagation with Zemax resulted in a loss of about 50% peak power loss compared to a Gaussian beam of the same size, but also to a negligible influence of wavefront planarity

This is currently being performed in a proof-of-concept demonstrator activity funded by ESA. Preliminary results show that the low received light likely requires a dedicated optimisation of the phase locked loop, including evaluation the achievable laser frequency noise, the achievable received power level and the input current noise of the photodetectors. Regarding straylight on the optical bench of the retroreflector scheme a reduction of the optical power of better than 10^{15} in a field of view of about 300 µrad is required between the transmit beam of the optical bench and the received measurement beam on PD2. As this is considered very demanding, the performed straylight analysis is currently being verified by test in the proof-of-concept demonstrator activity. For comparison, the corresponding straylight suppression requirement for the transponder scheme is 10^4 to 10^6.

The noise terms as stated in Table 3, Figs. 2 and 3 have individual frequency dependencies. Nonetheless, for simplicity we define the requirements breakdown for the individual contributors via the noise shaping function at a level that the performance is below the NSF for the whole required frequency range, resulting in a worst case assumption for the individual contributors. Figure 5 displays the proposed requirements breakdown of the instrument ranging noise and the current analysis result for both interferometer schemes. The figure shows the individual contributions from each unit and scheme in terms of allocation, and current best estimate (CBE). The individual contributions are added up via RSS, as they are considered independent from each other. In addition, a worst case (WC) based on the individual CBEs is given to get a 'realistic worst case'. For this the individual contributions are all added up linearly. The contributions of the two spacecraft differ from each other due to the master/slave (in the case of the transponder) and active/passive side (in the case of the retroreflector) instrument setup. To arrive to single link noise from the single spacecraft noise contribution, the two SCs contributions are added up (RSS, LIN) and divided by two (see the two upmost levels of Fig. 5).

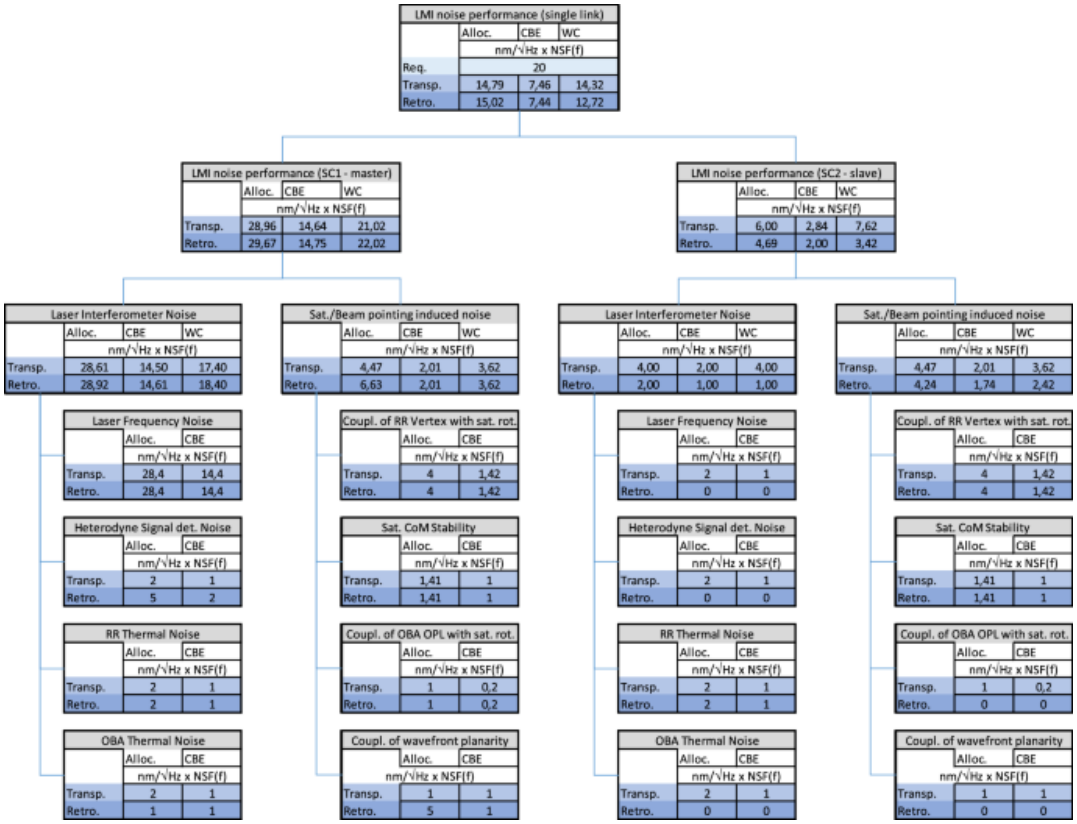

Fig. 5 LMI ranging noise breakdown

In summary, according to the current analysis, the two LMI schemes show very similar ranging noise performance, below the goal of 10 nm/√Hz × NSF(f) for the CBE and below the 20 nm/√Hz × NSF(f) for the 'realistic worst case'. Key contributor to the ranging noise for both schemes is the laser frequency noise. Compared to GRACE Follow-On, in which the main instrument noise contributors are the laser frequency noise, the satellite pointing noise and the thermally induced ranging noise, the performance improvement is achieved mainly due to the better thermal environment, reduced pointing noise of the satellites and the reduced inter-satellite distance.
The shorter inter-satellite distance between the satellites, if from one hand has a benign impact on the laser frequency noise, it has the disadvantage to reduce the sensitivity of the gravimeter arm with respect to the lower frequencies of the gravitational signal: but this drawback does not impact the scientific objectives of the mission, as assessed and collected in [19].

5 Link acquisition

For the heterodyne phase measurement of the LMI it is required that the laser beams of the satellites point to the other spacecraft better than roughly the beam divergence of about 150 µrad. If the pointing error is larger, the signal-to-noise-ratio drops below the detection capability of the photoreceivers and the phasemeter. Above this value, the received signal level is too low to detect a beat note due to received laser power and heterodyne efficiency for two superimposed beams with different propagation angles. In addition the laser frequency offset needs to be in the detection bandwidth of the photoreceivers and phasemeter, which is in the range of some MHz (at GFO LRI it is 4–18 MHz, for NGGM LMI 1–2 MHz are foreseen). The initial offset frequency uncertainty for the transponder scheme is assumed up to 1 GHz. For the retroreflector scheme, the offset frequency is given by the frequency shifter in the needed range.
The Attitude and Orbit Control System (AOCS) based on star cameras is expected to control the spacecraft to 100 µrad accuracy, but the initial alignment of the optical benches with respect to the satellite-to-satellite direction is expected to be limited to some mrad due to on-ground misalignments, one-g to zero-g effects, launch setting effects and to the knowledge error of the satellite relative

position in orbit. To achieve the initial link acquisition (and potentially later re-acquisitions), it is, therefore, needed to reduce the initial pointing uncertainty in advance.
In GRACE FO a fine steering mirror on both satellites is used to scan a field of view of about 3 mrad and to simultaneously scan one of the laser frequencies until both the pointing and the laser offset frequency are the same [24]. This approach was decided, as the GRACE FO spacecraft pointing control is rather coarse with approx. 2 mrad absolute pointing accuracy and a ± 300 µrad pointing jitter over the whole mission (limited by the on/off cold gas thruster control). It is a potentially rather lengthy and complex 5-dimensional scan (two spacecraft orientations and laser frequency sweep). The fine steering mirrors on GRACE FO are located on the optical benches and are voice coil based, requiring drive electronics and individual calibration activities. The satellite pointing noise is one of the main noise contributors to the LRI in GRACE FO (about the same as the laser frequency noise in the low frequency range).
For NGGM a much better satellite pointing control is foreseen by use of throttable electric thrusters, allowing an absolute pointing down to few µrad after initial calibration and using the LMI DWS signal as sensor. As alternative to steering mirrors on the optical benches, a dedicated acquisition light system is conceived, as shown in Fig. 4, consisting of the “acquisition light source” (ALS) and the “acquisition light detector” (ALD). This approach reduces the number of elements in the optical path, simplifies the optical bench, reduces electrical power demand in science mode and leads to a higher reliability as the acquisition light system can be implemented redundant. Furthermore, it simplifies the acquisition procedure, as it eliminates 4 dimensions of the initial acquisition process compared to GRACE FO. Once ALS and ALD are activated, the ALD immediately detects the direction of the other spacecraft, as the ALS acts as an ‘artificial guide’ star for the other satellite.
The ALS consists of a laser source with about 100 mW of output power, a beam divergence > 3 mrad and a wavelength optimized for the ALD spectral sensitivity, e.g., a single emitter fiber coupled laser diode. The ALD consists of an angle detector based on a position sensing detector (already breadboarded by Thales Alenia Space Italy) or on a pixel array sensor, allowing for higher accuracy at lower signal levels [18].
In the following, the link acquisition approach is described in detail for both the investigated LMI schemes.

5.1 LMI transponder scheme

For the transponder scheme the initial pointing uncertainty is assumed within ± 3 mrad and frequency offsets within ± 1 GHz. Figure 6 left shows an illustration of the acquisition procedure. To reduce the initial pointing uncertainty based on star camera measurements, the ALS/ALD systems are turned on simultaneously on both spacecraft and the AOCS is using the ALDs to turn the optical axes of the spacecraft to each other to less than 100 µrad accuracy (in pitch and yaw, roll remains controlled by the star cameras with relaxed AOCS requirements). Once the 100 µrad pointing accuracy are reached, the slave laser frequency is swept until the photoreceivers see a heterodyne signal (which should happen on both S/C at the same time), then the slave laser frequency is phaselocked to the master laser frequency. The ALS/ALD system can then be turned off and the spacecraft attitude angles are controlled via the DWS signal for the whole mission when in science mode.

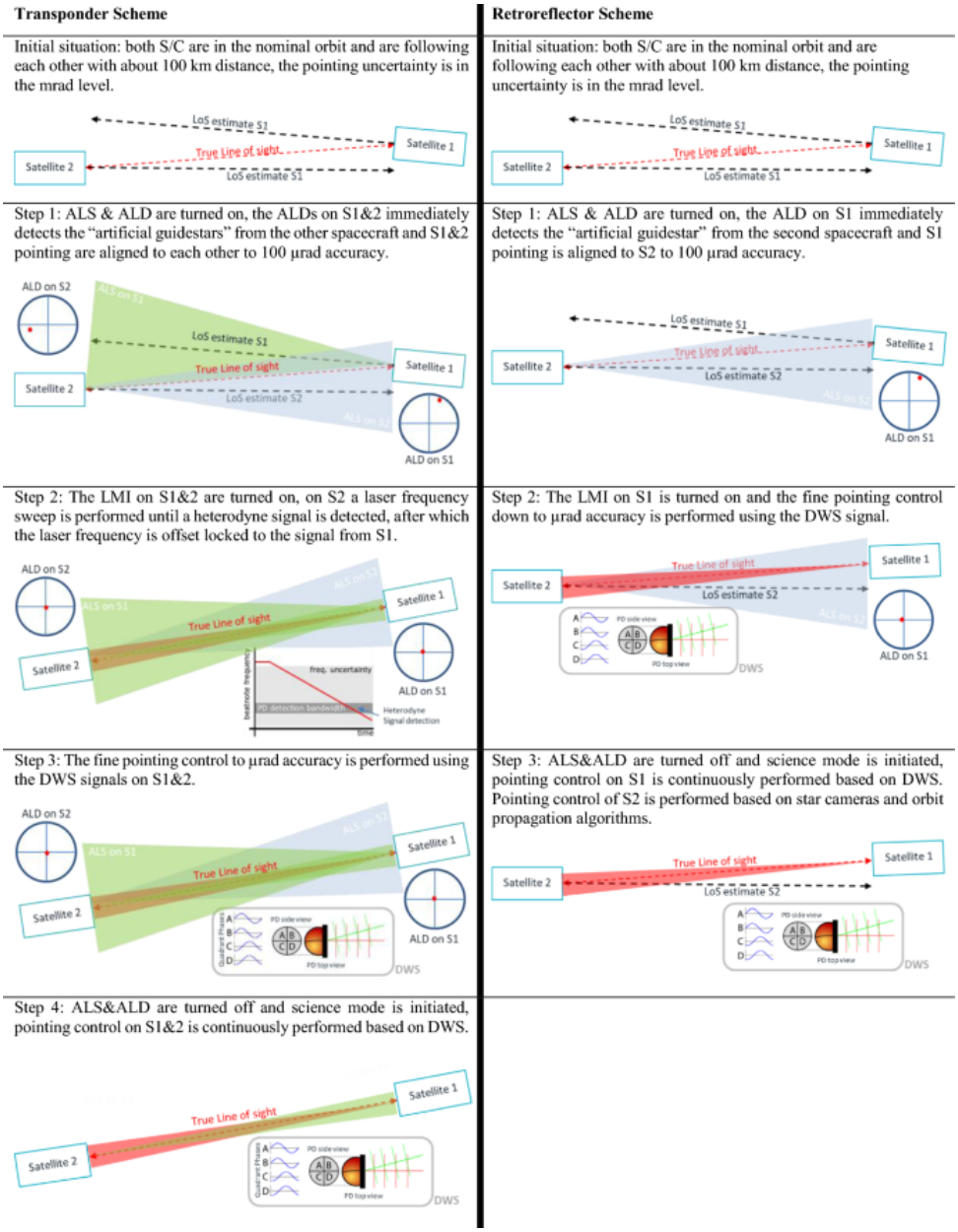

Fig. 6 Link acquisition. Left: LMI transponder scheme; Right: LMI Retroreflector Scheme

5.2 LMI retroreflector scheme

For the retroreflector scheme the initial pointing uncertainty is equally assumed within ± 3 mrad. The retroreflector scheme has only one LMI on one satellite active at any time, while on the second S/C only the passive retroreflector is used. The offset frequency is set by the frequency shifter on the active S/C. Therefore, the initial acquisition procedure is simpler.

To reduce the initial pointing uncertainty the ALS on the passive spacecraft is turned on as well as the ALD on the active side. The attitude control system on the active S/C is using the ALD to point the optical axes of the spacecraft to the second S/C to less than 100 µrad accuracy in pitch and yaw, as well roll remains controlled by the star cameras with relaxed AOCS requirements. On the passive side, the 3 mrad pointing accuracy are sufficient when the baffle diameters are designed accordingly. However, also on the passive spacecraft, the pointing noise in the measurement band needs to be as good as on the active side. The AOCS based on star cameras in combination with the angular rate measurement of the accelerometers is able to achieve the required performance.

Once the 100 µrad accuracy is reached, the photoreceiver on the active S/C sees a heterodyne signal and the DWS sensor can be used. The ALS/ALD system can then be turned off and the

spacecraft attitudes are controlled via the DWS signal for the whole mission when in science mode. Figure 6 right shows an illustration of the acquisition procedure.

6 Reliability assessment and preliminary redundancy assessment

The reliability for the LMI has been required to be at least 87% for the mission design lifetime of 7 years, as a typical requirement for Earth observation missions. A first reliability assessment of the LMI schemes has been performed based on available or assessed 'Failures In Time' (FIT) values of individual components and assemblies. The reliability calculation is following the required approach according to ECSS–Q-HB-30-08A. Table 4 lists the utilized formulas for the calculation, taken from [25].

Table 4 Reliability calculation formulas [25]

Parameter	Formula
Component reliability	$R(t) = e^{-\lambda_{hour} \cdot t} = e^{-\frac{FIT}{10^9} T}$ with t = the mission time
Failure rate	$\lambda_{hour} = \frac{X^2(\alpha,\nu)}{2T}$ with T = Time of operation (Number of tested devices x test time x acceleration factor) $X^2(\alpha,\nu)$ = probability function Chi-squared for the number of failures, with α = confidence level (for reliability calculation $\alpha = 0.6$ is used) and $\nu = 2*r+2$ with r = number of failures during test
Failures in time FIT	$FIT = \lambda_{hour} \cdot 10^9 \rightarrow \lambda_{hour} = \frac{FIT}{10^9}$ $FIT^* = -\frac{10^9 \cdot \ln R(T)}{T}$
Reliability for serially connected elements	$R_{series}(t) = \prod_{i=1}^{n} R_i(t)$
Reliability for parallel elements	$R_{parallel}(t) = 1 - \prod_{i=1}^{n} (1 - R_i(t))$

To calculate the reliability of any system for any lifetime, the FIT values for all elements are needed. Table 5 states the assessed FIT values for the key LMI components. Please note that, based on the current development phase before mission adoption, these figures are partly rough estimations taken from other developments or generic current best estimates: further design iteration might influence these values. Purely mechanical and simple opto-mechanical elements (e.g., optical plates in mount) are considered to have a low FIT value (1–10) achieved by proper design.

Table 5 FIT value assumptions for key LMI components (MERLIN FRU is referring to the Optical Frequency reference unit of the MERLIN mission that is currently being developed at STI)

Component	UNIT	FIT	Component's Reliability for mission	Failure probability during mission	FIT Assessment Source
Power Electronics	ICU, LH	482	97,1%	2,9%	MERLIN FRU
FPGA Board	ICU, LH	182	98,9%	1,1%	MERLIN FRU
Backplane	ICU	47	99,7%	0,3%	MERLIN FRU
ECDL Seeder	LH	1000	94,0%	6,0%	CBE assessment, generic
Seeder Current drivers (2xLD 2XTEC)	LH	392	97,6%	2,4%	MERLIN FRU
Fiber Amplifier (Optical part)	LH	200	98,8%	1,2%	CBE assessment, generic
Amplifier Pump diodes (incl. Drivers)	LH	921	94,5%	5,5%	MERLIN FRU (DFB Diodes)
AOM incl. Driver	LH	500	97,0%	3,0%	CBE assessment, generic
EOM Driver (Cavity)	LH	250	98,5%	1,5%	CBE assessment, generic
Optical Cavity alignment	CAV	50	99,7%	0,3%	CBE assessment, generic
Photoreceiver	CAV	643	96,1%	3,9%	MERLIN FRU
EOM	CAV	250	98,5%	1,5%	CBE assessment, generic
Optical System	CAV	50	99,7%	0,3%	CBE assessment, generic
Fiber splices	CAV	50	99,7%	0,3%	MERLIN FRU, 10 per splice
Fiber collimator	OBA	10	99,9%	0,1%	estimate, GFO design
Opto-mechanics	OBA	100	99,4%	0,6%	CBE assessment, generic
PD1 Quadrant-Photoreceiver + Preamp	OBA	800	95,2%	4,8%	MERLIN FRU (non quadrant)
Waveplate-mechanism (incl. Electronics)	OBA	623	96,2%	3,8%	Mech: Sentinel 5 CAS, el. CBE
RR Optomechanical Setup	RR	50	99,7%	0,3%	CBE assessment, generic

Utilizing these assumptions and performing the reliability calculation for fully non-redundant LMIs results in a reliability of approx. 59–69% for the transponder and retroreflector scheme, respectively. This is clearly below the required reliability. Therefore, we performed optimizations of both schemes to increase reliability, while at the same time considering the impact on total mass, required

mechanical envelops and costs, not only for the LMI but also the impact on the satellite as a whole. As can be seen below, this leads to two different approaches in terms of what kind of redundancy is implemented. The ALS and ALD are not included in the reliability analysis, because they are not formally considered part of the LMI from a system perspective.

6.1 LMI transponder scheme

For the transponder scheme, a partial redundancy of critical equipment is proposed as baseline. In this approach all high FIT valued components (such as: Electronics, Laser sources and Photoreceivers) are implemented in cold redundancy. Redundant units (and in some case components of the units) can be cross linked in case of a failure. A specific approach is proposed for the cavity: it is not redundant on one spacecraft. Cavity redundancy is achieved by flying one cavity on each spacecraft while needing only one at a time and the possibility to exchange the master and slave operational modes. The fibre connection of the LH to the OBA is foreseen to be cold redundant, with a beam superposition achieved via polarisation and a motorized halfwave-plate for polarisation control. The quadrant photoreceivers on the optical bench can operate in hot or cold redundancy. Figures 7 and 8 show the proposed instrument implementation and redundancy logic. Single string/non-redundant components are shown in the reliability logic as single boxes of the "chain of components", redundant components are shown above each other, the connection lines show potential crosslinking of the components. Using the component reliabilities stated in Table 5, the reliability for this configuration is calculated at 95% for the full mission duration. Only the opto-mechanical parts(optics and mounts) of the OBA and RR are implemented as non-redundant as they—following the mechanical design rules and associated design margins—are assessed with low FIT values. The full redundancy at component and unit level for the LMI is not deemed necessary, on the basis of this design and reliability calculation above.

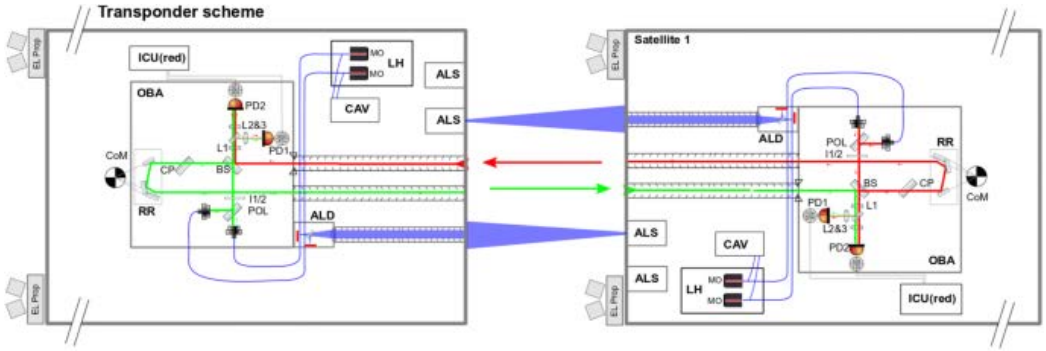

Fig. 7 Transponder scheme with partial redundancy

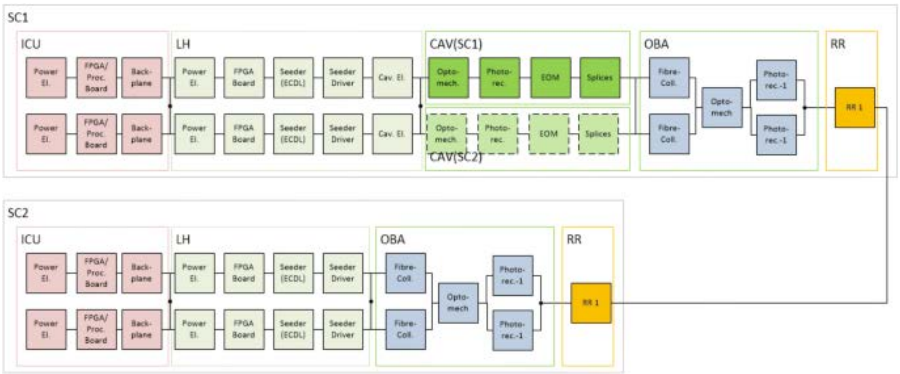

Fig. 8 Transponder scheme reliability logic

6.2 LMI retroflector scheme

For the retroreflector scheme it is proposed to implement an instrument level redundancy by having the identical instrument configuration on both spacecraft. The setup on each spacecraft is (to a large

extend) single-string. In case of a critical component failure the spacecraft exchange positions and switch the active/passive role. Figures 9 and 10 show the foreseen redundancy logic for the retroreflector scheme.

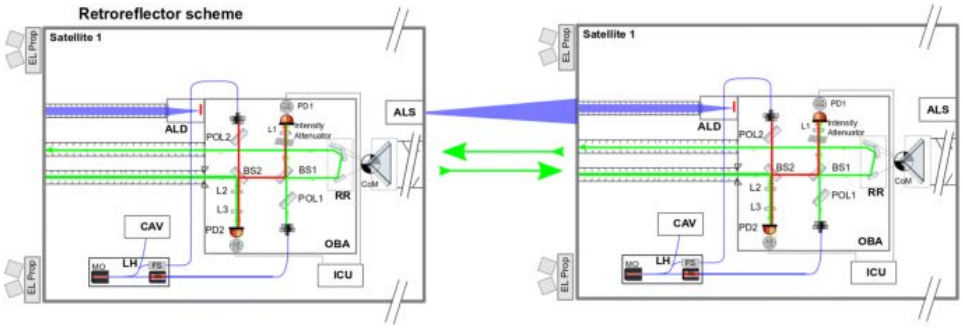

Fig. 9 Retroreflector scheme with full redundancy

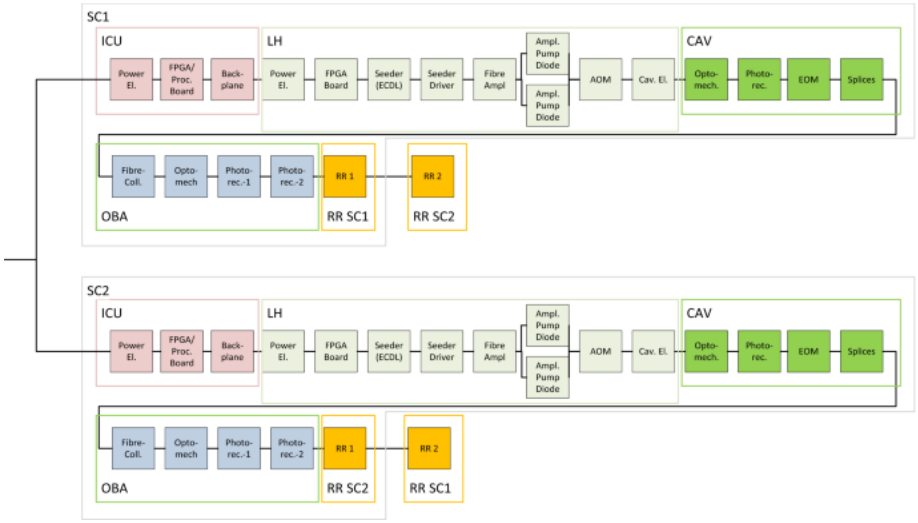

Fig. 10 Retroreflector scheme reliability logic

Compared to implementing partial redundancy as we propose for the transponder scheme, one benefit of this approach is that both satellites can be built identically, enabling for example a Proto Flight Model/Flight Model approach and associated to it a significantly reduced design and assemby, integration and test (AIT) effort compared to a solution with two different satellites. On the contrary, the alternative of implementing partial redundancy on the active instrument side would require a significantly higher mechanical envelope, make the optical bench even more complex and would lead to a significant asymmetry in the two spacecraft: therefore, is not proposed as the preferred baseline for NGGM. The reliability for this configuration calculates to 91% for the full mission duration.

Table 6 Reliability assessment of baseline LMI schemes for different mission durations

Criterion/parameter	Non-redundant	Proposed redundancy baseline	Enhanced redun-dancy
Transponder scheme	59%	95%	97.4%
Retroreflector scheme	69%	91%	98.6%

The results show that a partial redundancy with cross-linked units may have better reliability than a fully redundant instrument, where the individual units are not cross-linkable. The exact numbers are expected to change given the input data which need to be refined in parallel to the Phase A of the mission. The column 'enhanced redundancy' in Table 6 gives an indication of further options with higher redundancy by:

- Implementing the transponder scheme in 'symmetric' configuration, allowing the manufacturing of two identical spacecraft at the cost of about 20% more mass and volume requirement for the LMI. This is achievable by adding another optical bench, retroreflector and baffles and the required harness to the LMI, resulting in a similar configuration as the retroreflector scheme with respect to accommodation on the platform.
- Implementing the reflector scheme with added partial redundancy. For the retroreflector scheme, the involved units are the power electronics, the seed laser and the photoreceivers. The full redundancy of each string remains. The additional redundancy will lead to an increase of 10–20% on the mass and volume, but likely no significant effect on the required electrical power.

7 TRL assessment

The technology readiness level is an important criterion for the implementation of any satellite mission. Analysing the individual key units with respect to their technology readiness level, including the heritage from GRACE FO, former NGGM studies and LISA activities, a sound TRL assessment of the LMI units has been performed, on the basis of present and past activities and the NGGM system studies, e.g., [7, 8, 18, 20, 21, 26]. Table 7 lists assessments of the individual units of the LMI, also in comparison to GRACE FO. With the LMI consisting of a number of units individually mounted on the spacecraft, the TRL assessment focusses on these individual separate units. Given that at this phase of the development (pre-Phase A activities), most interfaces to the spacecraft are not fixed, the TRL statement excludes any necessary work to adapt the units to the final spacecraft accommodation (e.g., units that have flight heritage from GFO LRI are expected to be adapted for NGGM LMI). The authors consider this normal work but not critical.

Table 7 TRL assessment of the LMI units

Unit	Grace FO LRI (US and D)	Transponder scheme	Retroreflector scheme	Comment/unit provider
Instrument control unit	9 (US)	LISA:4 (−>6)	LMI: 3->4 LISA: 4 (−>6)	GFO: non-redundant, JPL [33] LMI: Proof of concept activity is running LISA: European Phasemeter breadboard exists [34]. EBB is planned to be developed
Laser head seeder Laser head amplifier	9 (D) –	NPRO: 9 ECDL: 4–5	NPRO: 9 ECDL: 4–5 Amplifier: 6	NPRO: Tesat RLH [7] ECDL: FBH MILAS [22, 28] Amplifier: HSL 2 activity in ESA [32]
Cavity	9 (US)	5–6	5–6	GFO: JPL/Ball Aerospace [7] EU: HSL2 and OSRC activities in ESA [32]
Optical bench	9 (D)	9	LMI: 3−>4	GFO: STI [7, 12] LMI: Proof of concept activity is running
Retroreflector	9 (D)	9	9	GFO: STI [7, 12]

The baseline laser seed source is the fully qualified Reference Laser Head (RLH) from Tesat, which is used in EDRS and also used on GRACE FO [7]: this RLH is a NPRO with Nd:YAG as laser crystal. Recent developments in diode laser technology make diodes an attractive alternative with respect to power, efficiency, wavelength range, mass and cost for a multitude of missions. External cavity diode laser (ECDL) based Butterfly packages achieve 10 mW of optical output power, e.g., [27]. Microintegrated ECDL modules developed by Ferdinand Braun Institute Berlin (FBH) currently achieve up to 500 mW optical output power, have been successfully operated on several sounding

rockets and have demonstrated the required parameters for LISA and NGGM in the lab [22, 28]. Their TRL is assessed within TRL 4–5 and they would need to be developed further to be used for NGGM. These sources are also considered attractive for LISA, atomic clock and optical communication applications [29,30,31]. Therefore, the authors consider a further development of these module towards a European seed laser building block beneficial for a range of future missions. Within the LMI retroreflector design, a fiber laser amplifier is already under development [32], similar to the one being developed for LISA [28]. The qualification status for the frequency shifter (AOM) needs to be assessed. A potentially suitable and qualified device may be available from Gooch & Housego. The optical bench is currently being breadboarded by STI under a contract granted by ESA (named proof of concept activity in Table 7). As the phasemeter required for the LMI is much simpler than the LISA phasemeter, the LISA phasemeter TRL is applied here also for the LMI for NGGM.
For mission adoption and project implementation, a TRL 6 is required for all units. The key necessary developments for having an all European LMI qualified at TRL 6 at unit level concern the ICU, the optical bench, the cavity, and (as back-up for risk mitigation with regard to the NPRO) the ECDL seed laser. In addition, a LMI test campaign is considered necessary to achieve TRL6 at instrument level.

8 Summary

To further improve the measurement accuracy of the time-variable gravity field, ESA is investigating the concept of a 'Next generation gravity mission' (NGGM), consisting of two pairs of satellites and a heterodyne laser interferometer for inter-satellite ranging. Two alternative schemes for the laser metrology instrument (LMI) for NGGM have been established and investigated. The results of GRACE FO verify the achievability of the assumed lower level performance allocations for the off-axis LMI-transponder scheme, when the foreseen improved satellite pointing and temperature stability of the NGGM satellite platform are taken into consideration. We can, therefore, state that the scheme can meet both the ranging noise requirement and the goal. For the off-axis LMI-retroreflector scheme all investigated aspects indicate as well that both the requirement and the goal can be met. However, more verification steps are currently under investigation to be able to ensure full compliance, specifically with respect to straylight, multi-path suppression and potential cycle slip issues.
The laser link acquisition strategy is similar for both schemes with somewhat increased complexity for the transponder scheme.
The reliability assessment of the two schemes indicate a higher reliability for the partially redundant transponder scheme due to the possibility to crosslink individual units, compared to the need to switch to the redundant instrument (and exchange the spacecraft positions) in case of a unit failure in case of the retroreflector scheme. On the other hand, full redundancy in the retroreflector design ensures resilience to one-point failure issues on the LMI and simplifies the implementation and verification approach of two (almost) identical satellites. Depending on the ultimately required mission lifetime and reliability, both schemes offer the possibility of additional redundancy.
Accommodation of both schemes is very similar. A main difference consists in the possibility of implementing an identical configuration of the two spacecraft (leader and follower in the formation) with the retroreflector scheme of the laser interferometer, allowing for a reduced effort on satellite bus side. The symmetry between the two spacecraft is broken with respect to the flight direction in the case of the optical transponder scheme of the laser interferometer, unless the propulsion system is doubled or the LMI is itself implemented symmetrically at the cost of increased mass, envelope and cost.
The technology for the LMI-transponder case is mostly available from GRACE Follow On. Specific necessary modifications would be a higher redundancy and a dedicated link acquisition system. For the LMI-retroreflector scheme, a suitable laser head and an optical bench breadboard is under development, with TRLs between 4 and 6 currently. Summarizing the different aspects of the interferometer concept trade off, the authors consider both schemes feasible for NGGM. The transponder scheme is a 'safe' option, with the LRI configuration from GRACE FO being fully qualified and in operation in orbit. The retroreflector scheme, while requiring a more complex laser

head and optical bench and not being fully verified yet, offers the possibility to reduce the costs on the satellite bus by implementing two identical spacecraft. The low received power and the resulting high requirement on straylight, multipath suppression and potential cycle slipping as well as the cost impact on the satellites as a whole is still being further investigated for a final decision on the NGGM baseline.

References

1. Tapley, B.D., et al.: Contributions of GRACE to understanding climate change. Nat. Clim. Change. (2019). https://doi.org/10.1038/s41558-019-0456-2
2. Reigber, C., et al.: A high-quality global gravity field model from CHAMP GPS tracking data and accelerometry (EIGEN-1S). Geophys. Res. Lett. (2002). https://doi.org/10.1029/2002GL015064
3. Bouman, J., et al.: Satellite gravity gradient grids for geophysics. Nat. Sci. Rep. 6, 21050 (2016). https://doi.org/10.1038/srep21050
4. Bruinsma, S.L., et al.: ESA's satellite-only gravity field model via the direct approach based on all GOCE data. Geophys. Res. Lett. 41, 7508–7514 (2014). https://doi.org/10.1002/2014GL062045
5. Flechtner F. et al. Observation of the system Earth. ISBN 978-3-642-32135-1 https://www.springer.com/de/book/9783642321344. Accessed March 2020
6. Flechtner, F., et al.: What can be expected from the GRACE FO laser ranging interferometer for earth science applications? Surv. Geophys. 37, 453–470 (2016)
7. Abich, K., et al.: In-orbit performance of the GRACE follow-on laser ranging interferometer. Phys. Rev. Lett. 123, 031101 (2019)
8. Cesare, S., et al.: The European way to gravimetry: from GOCE to NGGM. Adv. Sp. Res. 57, 1047–1064 (2016)
9. W. Folkner et al. Laser frequency stabilization for GRACE-II. Earth science technology forum, Arlington, Virginia, June 22, 2010. https://trs.jpl.nasa.gov/handle/2014/41635. Accessed June 2020
10. Sheard, B.S., et al.: Intersatellite laser ranging instrument for GRACE follow-on mission. J. Geod. 86, 1083–1095 (2012)
11. Heinzel, G. et al. Laser ranging interferometer for GRACE follow-on. Proc SPIE 10564, International Conference on Space Optics—ICSO (2012) 1056420 (20 November 2017). https://doi.org/10.1117/12.2309099
12. Dahl, C. et al. Laser ranging interferometer on GRACE follow-on. Proc SPIE 10562, International Conference on Space Optics—ICSO (2016) 105623V (25 September 2017). https://doi.org/10.1117/12.2297705
13. Danzmann, K. et al. Laser interferometer space antenna. In: arXiv preprint arXiv: 1702.00786 18–20 (2017)
14. Gravitational observatory advisory team (GOAT). The ESA-L3 gravitational wave mission. Final report (4 May 2016). https://sci.esa.int/s/8Y6DKZA. Accessed June 2020
15. https://podaac.jpl.nasa.gov/datasetlist?ids=Collections:ProcessingLevel&values=GRACE-FO:*3*&search="GRACE-FO"&view=list
16. Haagmans, R., et al.: ESA's next-generation gravity mission concepts. Rend. Fi. Acc. Lincei. (2020). https://doi.org/10.1007/s12210-020-00875-0
17. Bender, P. et al. A possible dual-grace mission with 90 degree and 63 degree inclination orbits. In: Proceedings of the 3rd International symposium on formation flying, missions and technologies. ESA/ESTEC, Noordwijk 1–6 (2008)
18. Cesare, S. et al. Optical metrology for measuring Earth's gravity. In IEEE 5th International workshop on metrology for AeroSpace (MetroAeroSpace), Torino, Italy, 2019, pp. 495-499 (2019). https://doi.org/10.1109/MetroAeroSpace.2019.8869574
19. Pail, R., et al.: Science and user needs for observing global mass transport to understand global change and to benefit society. Surv. Geophys. 36(6), 743–772 (2015)
20. Laser Doppler interferometry mission for determination of the Earth's gravity field. ESTEC contract 18456/04/NL/CP, Final report, Issue 1 (2005)
21. Laser interferometry high precision tracking for LEO, ESA contract no. 2000512/06/NL/IA, Final report, (2008)
22. Bawamia, A., et al.: Semiconductor laser modules for precision spectroscopy applications in space. Proc. SPIE 11180, International Conference on Space Optics—ICSO 2018, 111805C (12 July 2019). https://doi.org/10.1117/12.2536111

23. Delgado, E. Laser ranging and data communication for the laser interferometer space antenna. PhD thesis, (Universidad de Granada 2012). https://hera.ugr.es/tesisugr/20761417.pdf. Accessed May 2020
24. Wuchenich, D., et al.: Laser link acquisition demonstration for the GRACE follow-on mission. Opt. Express. 22(9), 11351–11366 (2014). https://doi.org/10.1364/OE.22.011351
25. Ellermann, P. Calculating reliability using FIT and MTTF: Arrhenius HTOL model. MicroNote 1002; Rev 0, Microsemi, (2012)
26. Massotti, L., et al.: The ESA Earth observation programmes activities for the preparation of the next generation gravity mission. AIAA Guidance, Navig Control Conf 2013 Boston Mass (2013). https://doi.org/10.2514/6.2013-4637
27. https://www.rio-lasers.com/_products/1064nm-planex.html. Accessed March 2020
28. Dahl, K., et al.: A new laser technology for LISA. Int. Conf. Sp. Opt. (2019). https://doi.org/10.1117/12.2535931. (ICSO 2018, 111800C)
29. Hausschildt, H., et al.: ESAs ScyLight programme: activities and status of the high throughput optical network HydRON. Int. Conf. Sp. Opt. (2019). https://doi.org/10.1117/12.2535935. (ICSO 2018; 111800G)
30. Voland, C.: Towards optical data highways through the atmosphere. Free-Space Laser Commun XXXI (2019). https://doi.org/10.1117/12.2509648. (Proceedings volume 10910)
31. Frye, K. et al. The Bose-Einstein condensate and cold atom laboratory (2019). arXiv:1912.04849
32. Dahl, K., et al.: High stability laser for interferometric earth gravity measurements. Int. Conf. Sp. Opt. (2017). https://doi.org/10.1117/12.2296095. (ICSO 2016; 105620J 2017)
33. Bachman, B., et al.: Flight phasemeter on the laser ranging interferometer on the GRACE follow-on mission. J. Phys. Conf. Ser. 840, 012011 (2017)
34. Gerberding, O. et al. Breadboard model of the LISA phasemeter (2012). arXiv:1208.6418